Standardisation and Validation of Micro-CT for the Morphological Characterisation of Porous Structures

Greet KERCKHOFS, Jan SCHROOTEN, Martine WEVERS, Department of Metallurgy and Materials Engineering, Katholieke Universiteit Leuven, Leuven, Belgium
Philippe VAN MARCKE, Department of Geography-Geology, Leuven, Belgium
Tim VAN CLEYNENBREUGEL, Division of Biomechanics and Engineering Design, Katholieke Universiteit Leuven, Leuven, Belgium

Abstract. In order to understand and to simulate the functional behaviour of porous structures during loading, quantitative knowledge of the relationship between the morphology and the mechanical behaviour is necessary. Therefore, the porous structures need to be quantified morphologically. In this research, the quantification will be performed by using micro-CT. However, to date, this technique encounters some problems. Optimal acquisition parameters still need to be found by 'trial and error', which is subjective and time consuming. Additionally, there is a lack of quantitative validation criteria. Both problems are tackled in this study, where, at this point, titanium bone scaffolds are assessed as proof of principle.

By using a micro-CT simulator, theoretically optimal acquisition parameters are determined. These parameters are then used for the validation of micro-CT by means of metallographic slicing combined with optical microscopy. By matching the optical image with the micro-CT image of the same cross-section, validation criteria are defined. Based on three sliced parts of one Ti sample, a mean percentage in mismatch of 39.2 ± 7.8 % and in overlap of 75.6 ± 3.5 % with regards to the optical images is determined. To investigate whether these differences have a serious influence on the structural parameters, determined from the micro-CT images and the corresponding optical images, further image analysis is performed.

1. Introduction

Porous structures, for example filter materials, geological materials, bone and porous structures for bone replacement, so-called bone scaffolds, play an important role in everyday life. In order to understand and simulate the functional behaviour of these materials during loading, a thorough knowledge of the relationship between the morphology and the mechanical behaviour of such materials is necessary. This study focuses on the morphological characterisation of porous structures by means of microfocus X-ray computed tomography (micro-CT). This relatively young imaging technique visualises the three-dimensional, internal structure in a non-destructive way and is widely used in several material science disciplines [1-8].

Although micro-CT is extensively used, some problems arise when applied for the morphological quantification of porous structures. One bottleneck lies in finding the optimal acquisition parameters, such as the voltage, the current and the use of a filter. This is mostly done by trial and error, which is however subjective and time consuming. In addition, a lack of clear validation criteria hinders the assessment of porous structures such

as cellular foams, geological samples and bone scaffolds. At this point, a lot of ongoing research focuses on the validation of micro-CT for bone assessment using histology [9-13]. However, this validation is still not optimised and not applicable for all porous structures. Hence, an accurate morphological quantification of porous structures requires a standardisation and validation of micro-CT.

2. Materials and Methods

In this study a protocol for the optimisation and validation of micro-CT images is defined. Porous titanium bone scaffolds are used as an example material. Indicative values for optimal acquisition parameters are provided by a micro-CT simulator. These indicative values are the input for the physical visualisation of the bone scaffolds with micro-CT. Finally, a validation by comparison with metallographic slicing combined with optical microscopy is performed to quantify the accuracy of the micro-CT images. Validation criteria are defined based on the overlap and mismatch between the micro-CT and the optical images. Additionally, to investigate the influence of the mismatch, further image analysis is performed on both the micro-CT and the optical images.

2.1 Scaffold Materials

The samples used in this study are cylindrical Ti bone scaffolds (ø-h: 5-10 mm), produced by transforming Ti powder into open porous structures by gel casting [14-15]. The starting product is a stable suspension in which 25 vol% of the Ti-powder is dispersed in distilled H_20 with the aid of 3 wt% dispersion agent Targon 1128 or Dolapix PC33. When necessary, a thickener is added in order to obtain a stable suspension. For the gel casting technique, a foaming agent is added to the suspension and it is foamed by mechanically stirring during 10 minutes. After drying in air, the organic components are burned out at 600°C and the green structure is sintered. By altering the composition of the slurry and the stirring time, the pore diameter can be adjusted to obtain the desired pore size distribution. Altering the sintering temperature will influence the final mechanical and structural scaffold properties.

2.2 Micro-CT Equipment

In micro-CT, contrary to medical CT, the sample is rotated between a fixed X-ray source and a fixed detector. The source generates a polychromatic spectrum of X-ray intensities in function of the photon energies, which is dependent on the acquisition parameters. These parameters are the voltage, the current and the use of a filter, in front of the detector or right behind the source. The X-rays pass through the sample and during their passage, they are attenuated. The intensities of the attenuated X-rays are measured by the detector. By applying a mathematical algorithm on these detector measurements, grey-level images representing the attenuation inside the sample can be reconstructed. These resultant images are two-dimensional and show the geometry of the sample in the plane of the cross-section. A series of two-dimensional images can then be combined to create a three-dimensional representation.

For this study, two micro-CT devices are used. The characteristics of both devices are given in table 1.

Table 1: Characteristics of the two micro-CT devices.

	Philips HOMX 161 X-ray system with AEA Tomohawk CT-upgrade [165]	**Skyscan 1072 system [16-17]**
X-ray source	160 kV	130 kV
Maximum current	3.2 mA	77 µA or 300 µA
Microfocal spot	from 5 to 200 µm.	10 µm or 30-40 µm
Spatial resolution	minimum 10 µm	minimum 20µm
Detector	CCD camera with a resolution of 1024 x 1024 pixels and a 12 bit dynamic range	cooled CCD sensor with a resolution of 1024 x 1024 pixels and a 10 bit dynamic range
Maximum sample dimensions	about 20 cm width and 20 cm height	6 cm width and 6 cm height

2.3 Micro-CT Simulator

The acquisition parameters that give optimal images are determined by using a simulator for the Skyscan 1072 system. This simulator is a computer program simulating the real scanner [18]. It only applies for the acquisition process, no reconstruction algorithms are implemented. Reconstruction is performed after simulation, using the Feldkamp reconstruction algorithm [19].

The simulator is used to optimize the quality of the images obtained with the physical scanner and ensure an objective parameter selection, avoiding trail and error. The power of the simulator is that all acquisition parameters can be changed and their effect on the image quality can be investigated. This allows an efficient control for those acquisition parameters that result in optimal images for different materials and material morphologies.

The image quality is quantified based on three parameters: (i) presence of beam hardening, (ii) the contrast in the image and (iii) the focus of the image.

Beam hardening is an important artefact which occurs due to the absorption of the low energy X-rays at the edges of the sample. In this study, beam hardening is quantified by determining the absolute difference in intensity between two successive material peaks, starting from the edge of the sample. This method is visualised in figure 1. Peak A and B represent successive material peaks. The intermediate peaks do not represent material. Normally, all material peaks should have the same intensity because only one material is present in the sample. However, due to beam hardening, there can be a difference in peak intensities.

Due to the *contrast in the image*, a clear distinction can be made between the solid and the pores. To maximize the contrast, the pore-material intensity difference needs to be as high as possible. The contrast in the image is presented in figure 2. The material intensity is taken as the mean of the material intensities at the left and the right edge of the pore. Also for the pore intensity, an average is made between the air and the background noise intensity. In this image quality quantification, the contrast is always determined at the same location, thus it is only dependent on the acquisition parameters and not on the attenuation coefficient of the material.

The *focus of the image* implies the sharpness of the pore edges. If the edges are well-defined, the image is focussed. If not focussed, the edges are blurred, which can lead to the assumption of smaller pore sizes. The focus is quantified by determining the tangent of the pore edges in the image profile (red lines in figure 2). The steeper the tangent, the better the focus and hence, the better the image quality.

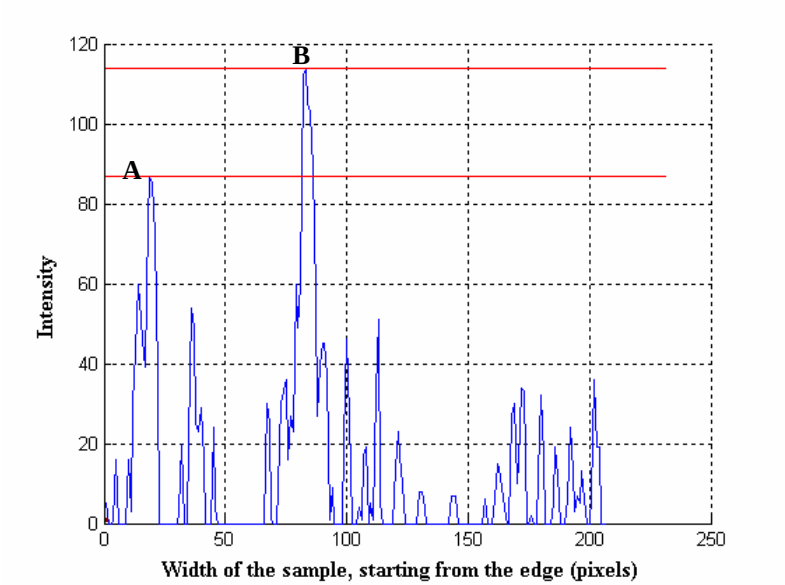

Figure 1: Profile of the material, generated at 110 kV and with a combination of an aluminium filter of 1 mm and a copper filter of 1 mm put right behind the source. Peak A represents the material at location A in figure 3a, peak B the material at location B.

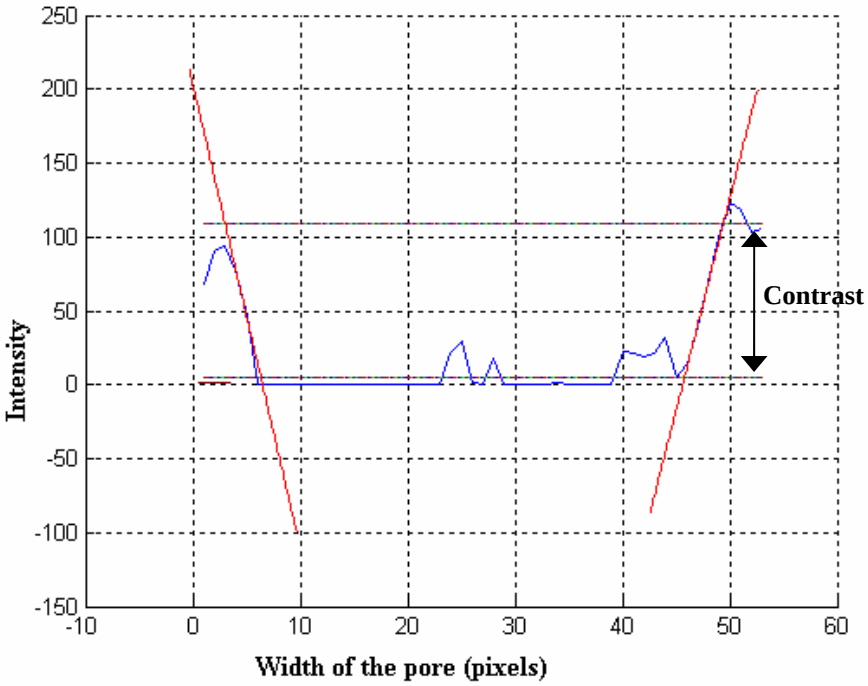

Figure 2: Intensity histogram of a pore of 70µm where the contrast is shown.

2.4 Validation of Micro-CT by Slicing Combined with Optical Microscopy

- Mismatch and overlap

To define validation criteria for micro-CT, comparison is made with a destructive imaging technique, namely slicing combined with optical microscopy. The validation procedure starts by generating micro-CT images of a complete titanium scaffold sample. The micro-CT device used for the validation is the Philips 161 HOMX system with AEA Tomohawk CT-upgrade, since this device is much more flexible to handle and the acquisition time is about 1/3th in comparison to the Skyscan 1072 system. Consequently, the acquisition parameters, determined by the micro-CT simulator, are used as *indicative* values.

Then, the sample is embedded in resin, cut in three pieces and the interfaces of the embedded sample are grinded and finally polished. These polished surfaces are visualised with an optical microscope and photographed at a magnification of 8. A full reconstruction of the surfaces is performed by stitching all images. These reconstructed optical images are segmented and binarized by manual thresholding.

After that, micro-CT images of the sliced samples are acquired. The same acquisition parameters as for the complete titanium sample are used. Subsequently, interpolated micro-CT images are extracted from the dataset of the complete sample by using the registration software of Maes et al. [21-22] and an interpolation software [23]. The interpolated micro-CT images are the images that lie in the plane where the sample was cut and thus, in the same plane as the optical images.

After registering the optical images to the corresponding interpolated micro-CT images, again by using the software of Maes et al., both are compared and matched visually by overlay. The amount of micro-CT image pixels, optical image pixels and overlap pixels are calculated in the overlaid images and the percentage in mismatch and overlap is determined. They are a measure for the accuracy of the micro-CT images. Percentage in mismatch is defined as the sum of pixels that belong to the micro-CT image and that are not overlap pixels, divided by the sum of the optical image pixels, taking into account the overlap pixels. Percentage in overlap is defined as the amount of overlap pixels divided by the total amount of optical image pixels, taking into account the overlap pixels.

It was found that the threshold of the interpolated micro-CT images influences the percentages in mismatch and overlap significantly. Hence, the optimal threshold is determined with an algorithm that minimizes the amount of pixels that belong to the optical and the micro-CT images and not to the overlap, and maximizes the amount of overlap pixels.

- Image analysis

Apart from defining validation criteria based on visual matching, comparison of five structural parameters from both the micro-CT and the optical images is performed. In this way, the influence of the mismatch is investigated. The structural parameters are calculated with the use of CTAn, an analysing software of Skyscan [24]. The five parameters, together with an explanation are given in table 2.

Table 2: Structural parameters, used for the validation of micro-CT.

Porosity	The volume that belongs to the pore space, divided by the total volume.
Specific surface of the pores	The pore space surface divided by the pore space volume = basic parameter in characterising the complexity of the structure.
Mean pore size (plate model)	The mean of the sizes of all the pores, calculated based on the plate model [25].
Mean polar moment of inertia	The number of solid pixels multiplied by their distance from the centre of gravity or centroid of a cross-sectional object. It is a basic strength index and indicates the resistance to torsional rotation of a cross-section.
Mean Fragmentation index	This is an index of connectivity of the pores, which was developed by Hahn et al. [26]

3. Results and discussion

3.1 Micro-CT Simulator

The input structure for the micro-CT simulator is presented in figure 3. Images are generated for voltages ranging from 40 kV to 120 kV and for three different filtering cases: F1 = no filter, F2 = an aluminium filter of 1 mm and F3 = a combination of an aluminium filter of 1 mm and a copper filter of 1 mm. All these filters are placed right behind the source. Figure 4 shows three images, generated by the micro-CT simulator at 40 kV and for the three filtering cases. As can be seen, a lot more noise appears in filtering case F3. A copper filter absorbs a high amount of the X-rays. In order to obtain a calibrated background, the exposure time has to double, resulting in a significant magnification of the amount of noise.

Beam hardening will be checked on path 1 and 2 (figure 5a). Both the *contrast* and the *focus* are determined for different pore sizes in the structure, ranging from about 70 µm at location 1 to about 6 µm at location 4 (figure 5b).

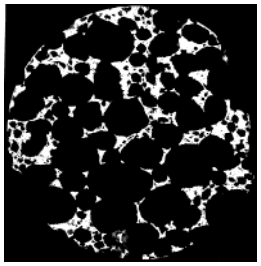

Figure 3: Input structure for the simulator.

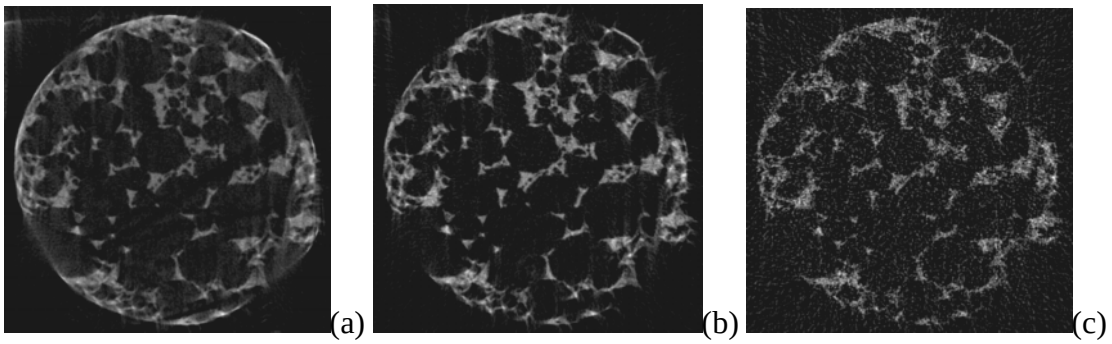

(a) (b) (c)

Figure 4: Theoretical images, at 40 kV, and the three filtering cases: (a) F1, (B) F2, (c) F3.

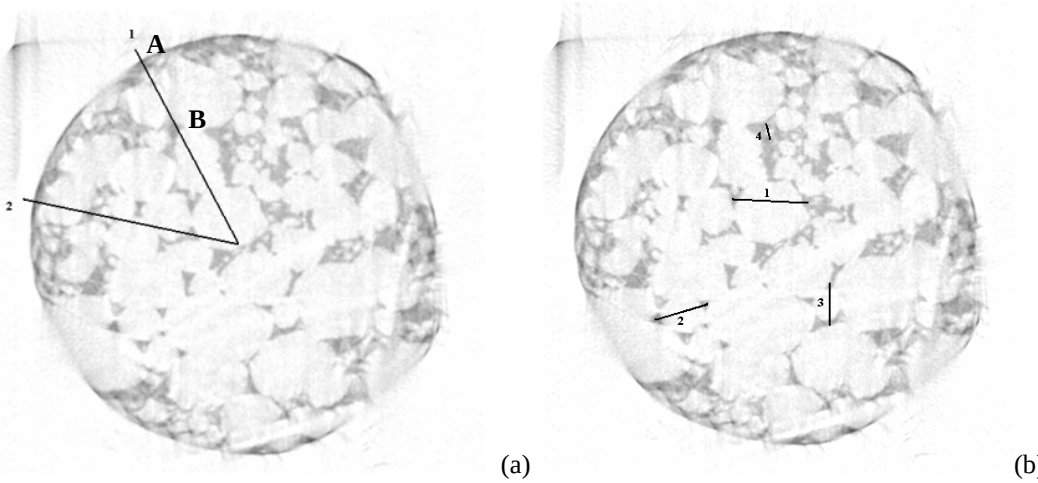

(a) (b)

Figure 5: (a) The beam hardening effect is checked on path 1 and path 2, (b) the contrast and the focus are determined at pores 1 to 4, ranging from large to small pore size.

Figure 6 gives a summary of the *beam hardening effect* at the different acquisition parameters along path 1 (figure 5a).

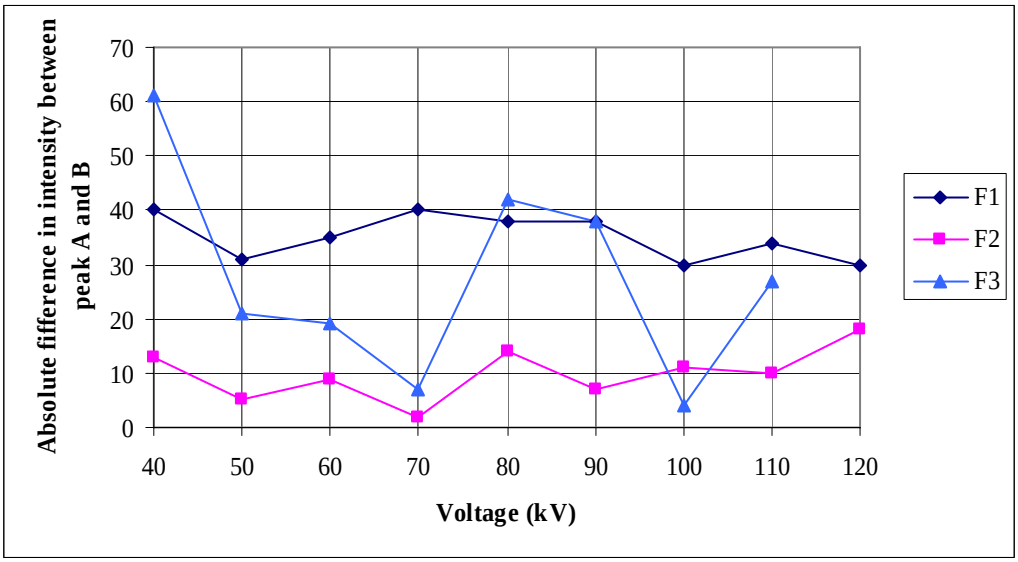

Figure 6: Influence of the acquisition parameters on the beam hardening effect

The smaller the absolute difference in intensity between peak A and B, the less pronounced the beam hardening effect. Thus, the aluminium filter of 1 mm (F2) shows the best results and no significant influence of the voltage is observed. The same conclusions are drawn for path 2 (figure 5a). Hence, when only focussing on the beam hardening effect, it can be concluded that the optimal voltage could range from 40 kV to 120 kV and that an aluminium filter of 1 mm shows the best results. It can also be seen that the higher amount of noise in filtering case F3 leads to significant fluctuations in the contrast curve.

Figure 7 shows the effect of the acquisition parameters on the *contrast* for a pore of about 70 µm (location 1 in figure 5b).

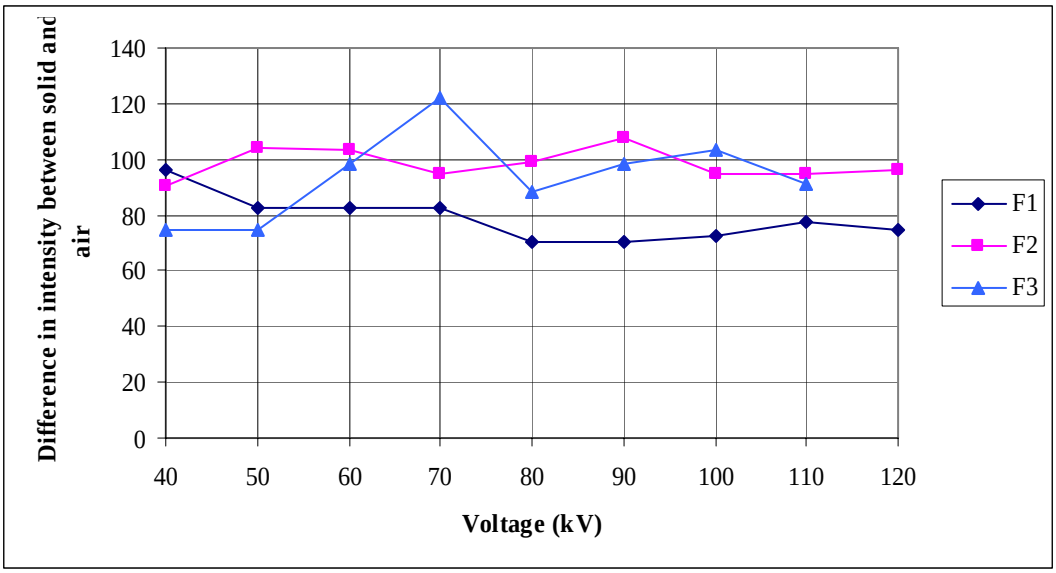

Figure 7: Influence of the acquisition parameters on the contrast for a pore of 70 µm

It is shown that the use of an aluminium filter of 1 mm (F2) increases the contrast. Also, when using this filter, the voltage has no significant influence on the contrast.

When comparing the contrast values at the different locations, it is noticed that the contrast at location 1 (pore size of 70 µm) is about 3 times higher than at location 4 (pore size of 6 µm). This phenomenon can be explained by the limited resolution of the Skyscan 1072 device. However, for the acquisition parameters the same conclusions apply for all locations. Thus, when only taking into account the contrast, optimal acquisition parameters could range from 40 kV to 120 kV and an aluminium filter of 1 mm should be used.

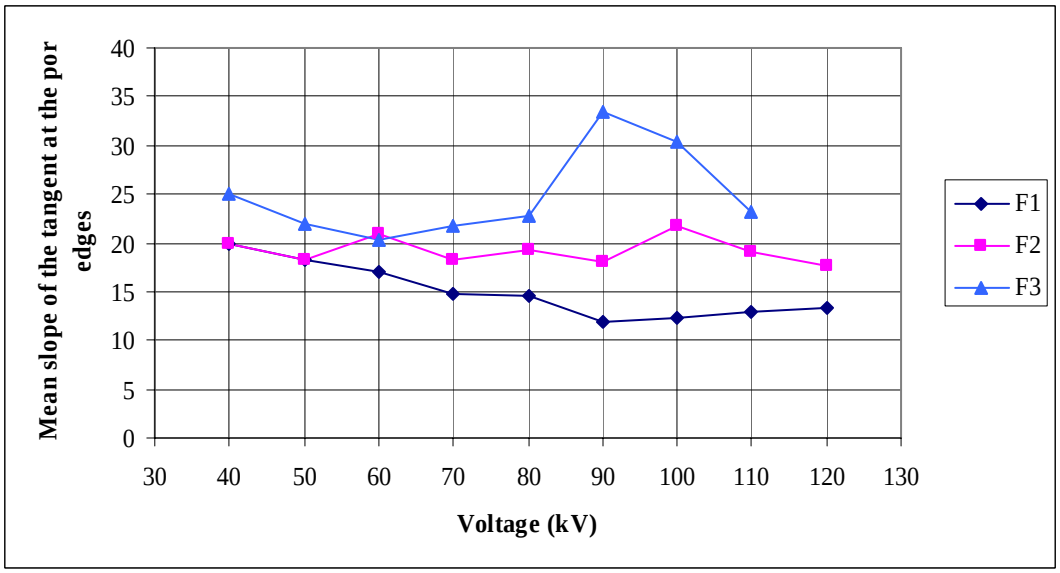

Figure 8: Influence of the acquisition parameters on the focus for a pore of 70 µm.

Figure 8 shows that a larger slope of the pore edges results in a better focus. Hence, filtering case F3 shows the best focus for a pore of about 70 µm. However, for the other pore sizes, filtering cases F1 and F2 keep the same trend, but filtering case F3 fluctuates significantly. Thus filtering case F2 is preferred due to its stable behaviour as function of the pore size. When only looking at the focus, voltages ranging from 40 kV to 120 kV should be applied and an aluminium filter of 1 mm should be used.

By combining all image quality parameters, it can be concluded that the optimal voltage for scanning titanium bone scaffolds ranges from 40 kV to 120 kV and that an aluminium filter of 1 mm should be used. However, when applying a voltage of 40 kV to 60 kV, the exposure time will be high and hence the scanning time goes up. Consequently, voltages ranging from 70 kV to 120 kV are preferred. Using the selected parameter values as indicative values, physical micro-CT imaging can now be performed.

3.2 Validation of Micro-CT by Slicing Combined with Optical Microscopy

- Mismatch and overlap

According to the optimal acquisition parameters, determined with the use of the micro-CT simulator, a voltage of 90kV is used for the acquisition of the complete Ti sample and the three sliced parts, and an aluminium filter of 1mm is placed right behind the source. The resulting images have a spatial resolution of 27µm, the images are averaged over 32 frames and random movement is allowed.

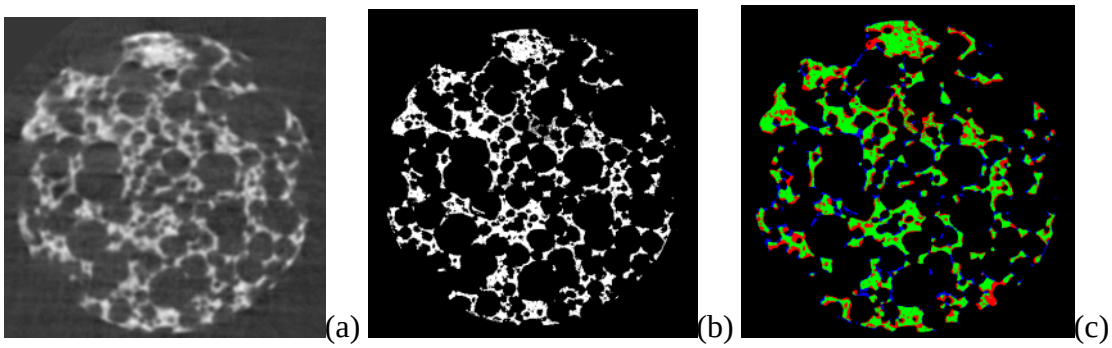

Figure 9: (a) Interpolated micro-CT image, (b) registered optical image and (c) overlap image of the sliced part Ti-A of a Ti sample.

Figure 9 shows the interpolated micro-CT image, the registered optical image and the overlap image of the sliced part Ti-A of a Ti sample. In the overlap image, red represents the micro-CT image pixels, blue the optical image pixels and green the overlap pixels. Calculations were made on one complete Ti sample and its three proper sliced parts, resulting in an average percentage in mismatch of 39.2 ± 7.8 % and an average percentage in overlap of 75.6 ± 3.5 %.

- Image analysis

Tables 3 to 5 give a summary of the structural parameters, calculated on both the micro-CT and the optical images, for the three different sliced parts of a Ti-samples (A, B and C).

Table 3: Structural parameters, calculated on the interpolated micro-CT image and the optical image, for sliced part Ti-A

	Micro-CT Ti-A	**Optical Ti-A**
Percent porosity (%)	78.13	79.95
Specific surface of the pores (1/µm)	0.0031	0.0032
Mean polar moment of inertia (µm^4)	1.44E+19	1.27E+19
Mean pore size (plate model) (µm)	651.43	624.71
Mean fragmentation index (1/µm)	-0.00020	-0.00067

Table 4: Structural parameters, calculated on the interpolated micro-CT image and the optical image, for sample Ti-B

	Micro-CT Ti-B	**Optical Ti-B**
Percent porosity (%)	79.04	82.47
Specific surface of the pores (1/µm)	0.0031	0.0032
Mean polar moment of inertia (µm^4)	1.33E+19	1.26E+19
Mean pore size (plate model) (µm)	649.01	632.97
Mean fragmentation index (1/µm)	-0.00036	-0.00081

Table 5: Structural parameters, calculated on the interpolated micro-CT image and the optical image, for sample Ti-C

	Micro-CT Ti-C	**Optical Ti-C**
Percent porosity (%)	74.32	74.77
Specific surface of the pores (1/µm)	0.0034	0.0037
Mean polar moment of inertia (µm^4)	1.00E+19	1.53E+19
Mean pore size (plate model) (µm)	653.4885	630.6949
Mean fragmentation index (1/µm)	-7.30E-05	-0.00048

As expected, the porosity of the optical images is slightly higher than that of the micro-CT images. The reason is found in the limited resolution of the micro-CT images. They overestimate the structure, resulting in a lower porosity. The same explanation can be given to the lower specific surface of the pores and the larger mean pore size for the micro-CT images. Due to the limited resolution, very small pores are not taken into account and hence, the mean pore size is larger for the micro-CT images. The mean fragmentation indices are for all cases very small and negative, which implies a high connectivity of the pores. The effect of the mismatch on these four parameters is not significant. A mean difference in porosity of 2.3 ± 1.8 %, in specific pore surface of 4.8 % 2.9 % and in mean pore size of 3.5 ± 0.9% is achieved when using micro-CT instead of optical microscopy.

However, the mean polar moment of inertia suffers from the mismatch. Due to the limited resolution of the micro-CT images, very small micropores are not taken into account, and this has significant influence on the calculation of the mean polar moment of inertia.

3.3 Discussion

The micro-CT simulator has provided a range of indicative optimal acquisition parameters for generating micro-CT images of the titanium bone scaffolds. Based on the presence of beam hardening, the contrast in the image and the focus of the image, it was decided that a voltage ranging from 40 kV to 120 kV should be applied and an aluminium filter of 1 mm should be placed right behind the source. However, when taking the acquisition time into account, the range of voltages was narrowed starting from 70 kV to 120 kV. Based on these conclusions, micro-CT images were generated for the validation of the technique combined with metallographic slicing and subsequent optical microscopy. By overlaying the optical image and the interpolated micro-CT image in the same plane, a percentage in mismatch and in overlap was determined. Calculations on the three sliced parts of one Ti sample resulted in an average percentage in mismatch of 39.2 ± 7.8% and in overlap of 75.6 ± 3.5 %. Since this mismatch was significant, image analysis was performed on both the micro-CT and the optical images to evaluate the influence of the mismatch on the structural parameters. This resulted in a mean difference in porosity of 2.3 ± 1.8 %, in specific pore surface of 4.8 ± 2.9 % and in mean pore size of 3.5 ± 0.9% with respect to the optical images. Although these values show interesting results, still an exhaustive validation should be performed on a large set of Ti samples, as well as on other materials. Ti samples were used as a proof of principle.

4. Conclusions

This study wanted to provide a protocol for the optimisation of the acquisition and the validation of micro-CT images. First, a micro-CT simulator was used for investigating the influence of the acquisition parameters on the image quality. Based on the presence of beam hardening, the contrast in the image and the focus of the image, indicative values for optimal acquisition parameters for Ti scaffolds were determined. This eliminates finding the optimal acquisition parameters by trial and error. The optimal acquisition parameters were used as indicative values for the acquisition of the micro-CT images which were applied for the validation of micro-CT by metallographic slicing combined with optical microscopy. A systematic procedure for this validation was produced, resulting in a definition of a mismatch and an overlap with regard to the optical images. Additionally, to investigate the influence of the mismatch on the calculation of the structural parameters, image analysis was performed on both the micro-CT and the optical images.

5. Acknowledgements

This work is done in collaboration with the Guided Bone Engineering project, an interdisciplinary research project funded by IWT-Flanders under the programme for strategic basic research (GBOU-020181).

References

[1] Ketcham, R.A. et al., *Acquisition, optimization and interpretation of X-ray computed tomographic imagery: applications to the geosciences,* Computers & Geosciences, 2001, **27**(4): p. 381-400.

[2] Schantz, J.T., et al., *Application of an X-ray microscopy technique to evaluate tissue-engineered bone-scaffold constructs,* Materials Science & Engineering C-Biomimetic and Supramolecular Systems, 2002, **20**(1-2): p. 9-17.

[3] Buffiere, J.Y., et al., *Damage assessment in an Al/SiC composite during monotonic tensile tests using synchrotron X-ray microtomography,* Materials Science and Engineering a-Structural Materials Properties Microstructure and Processing, 1997, **234**: p. 633-635.

[4] Bastawros, A.F. et al., *Experimental analysis of deformation mechanisms in a closed-cell aluminum alloy foam,* Journal of the Mechanics and Physics of Solids, 2000, **48**(2): p. 301-322.

[5] Blacher, S., et al., *Image analysis of the axonal ingrowth into poly(D,L-lactide) porous scaffolds in relation to the 3-D porous structure,* Biomaterials, 2003, **24**(6): p. 1033-1040.

[6] Maire, E., et al., *In situ X-ray tomography measurements of deformation in cellular solids,* Mrs Bulletin, 2003, **28**(4): p. 284-289.

[7] Lim, K.S. and M. Barigou, *X-ray micro-computed tomography of cellular food products,* Food Research International, 2004, **37**(10): p. 1001-1012.

[8] Maire, E., et al., *X-ray tomography applied to the characterization of cellular materials. Related finite element modeling problems,* Composites Science and Technology, 2003, **63**(16): p. 2431-2443.

[9] Fajardo, R.J., et al., *Assessing the accuracy of high-resolution X-ray computed tomography of primate trabecular bone by comparisons with histological sections,* American Journal of Physical Anthropology, 2002, **118**(1): p. 1-10.

[10] Chappard, D., et al., *Comparison of eight histomorphometric methods for measuring trabecular bone architecture by image analysis on histological sections,* Microscopy Research and Technique, 1999, **45**(4-5): p. 303-312.

[11] Mitton, D., et al., *Mechanical properties of ewe vertebral cancellous bone compared with histomorphometry and high-resolution computed tomography parameters,* Bone, 1998, **22**(6): p. 651-658.

[12] Cortet, B., et al., *Relationship between computed tomographic image analysis and histomorphometry for microarchitectural characterization of human calcaneus,* Calcified Tissue International, 2004, **75**(1): p. 23-31.

[13] Stoppie N., et al., *Validation of microfocus computed tomography in the evaluation of bone implant specimens,* Clinical Implant Dentistry and Related Research, 2005, 7(2): p. 87-94

[14] Snijkers, F., et al., *Porous Materials as Scaffold for Bone Replacement,* Acers-meeting Cocoa Beach, January 2005, Florida, USA
[15] S. Impens, et al., *Production and characterization of CaP en Ti scaffolds for bone tissue engineering*, 19th European Conference on Biomaterials, September 11-15 2005, Sorrento, Italy
[16] http://www.mtm.kuleuven.ac.be/Research/NDT/MicrofocusCT/index.html
[17] http://www.skyscan.be
[18] De Man, B. *Iterative reconstruction for reduction of metal artefacts in computed tomography*, PhD thesis, 2001, K.U.Leuven, Belgium.
[19] Feldkamp LA, et al., *Practical cone-beam algorithm*, Journal of the Optical Society of America A, 1984, **1**(6): p. 612-619.
[20] Maes F., et al., *Medical image registration using mutual information*, Proceedings of the IEEE, 2003, **91**(10): p. 1699-1722
[21] Maes F., et al., *Multimodality image registration by maximization of mutual information*, IEEE transactions on Medical Imaging, 1997, **16**(2): p. 187-198
[22] Personal communication with Ir. Gabriel Kiss
[23] http://www.skyscan.be/next/downloads.htm
[24] Parfitt AM, et al., *Bone Histomorphometry: standardization of nomenclature, symbols and units*, Journal of Bone and Mineral Research, 1987, **2**(6): p. 595-610.
[25] Hahn M, et al., *Trabecular bone pattern factor – a new parameter for simple quantification of bone microarchitecture*, Bone, 1992, **13**: p. 327-330.